Simulating Cyclohexane Millisecond Oxidation: Coupled Chemistry and Fluid Dynamics

R. P. O'Connor and L. D. Schmidt
Dept. of Chemical Engineering and Materials Science, University of Minnesota, Minneapolis, MN 55455

O. Deutschmann
Heidelberg University, IWR, I.N.F. 368, D-69120 Heidelberg, Germany

Cyclohexane partial oxidation over a 40-mesh Pt−10%Rh single-gauze catalyst can produce ~85% selectivity to oxygenates and olefins at 25% cyclohexane conversion and 100% oxygen conversion, with cyclohexene and 5-hexenal as the dominant products. A detailed 2-D model of the reactor is solved using density-functional theory (with 35 reactions among 25 species) and computational fluid dynamics. Rapid quenching in the wake of the wires allows highly nonequilibrium species to be preserved. The simulations show that the competition between cyclohexyl and cyclohexylperoxy radicals is crucial in determining product selectivities. At high temperatures and low pressures, the cyclohexyl radical is favored, leading to high selectivities to cyclohexene. At lower temperatures or high pressures, cyclohexylperoxy radicals are favored, allowing the formation of parent oxygenates to dominate. Numerical simulations suggest ways to tune reactor operation for desired product distributions and allow the investigation of dangerous or costly operating conditions, such as high pressure.

Introduction

Cyclohexane oxidation is a major process in the chemical industry. Over 90% of the cyclohexane used annually is oxidized to produce intermediates for the production of polymers, mostly nylon 6 and 6,6. These nylon intermediates include cyclohexene, cyclohexanone, cyclohexanol, and adipic acid. The production of these chemicals is characterized by exceedingly long residence times (~ 1 h) and inefficiencies of size, operating costs, and energy usage (and therefore emissions).

In recent years, millisecond reactors employing Pt−10%Rh single-gauze catalysts have shown promise for high-throughput and autothermal production of oxygenates and olefins (Goetsch et al., 1996; Iordanoglou et al., 1999; O'Connor and Schmidt, 2000a,b). In particular, cyclohexane oxidation over a single-gauze catalyst can produce > 80% selectivity to oxygenates and olefins at 25% cyclohexane conversion and 100% oxygen conversion, with a residence time six orders of magnitude smaller than that for comparable liquid-phase industrial processes. Close to 60% selectivity to cyclohexene and the 1,6-difunctional oxygenated species 5-hexenal can be achieved. Cyclohexene is more valuable than cyclohexane, and synthesis of cyclohexanone from cyclohexene is relatively simple. 5-Hexenal is an end-functionalized olefinic aldehyde, also potentially useful for the synthesis of polymers.

This one-stage autothermal reactor, with a single gauze layer of 18-mm diameter, can process ~ 8 kg/d of cyclohexane and produce 5-hexenal and cyclohexene with carbon yields of ~ 0.55 kg/d and ~ 0.65 kg/d, respectively, at a pressure of 2 atm. Direct scale-up to a reactor with a gauze of 1-m diameter at a constant time and no recycle should give ~ 5,000 kg/d of a mixture of 5-hexenal and cyclohexene. Such a blend could be used for the manufacture of nylons or novel polymers. Both cyclohexene and 5-hexenal can potentially be converted to adipic acid for the production of nylon 6,6. Poly(5-hexenal) could be an interesting polymer with unique properties arising from the large oxygen-containing side groups [$-(CH_2)_3CH=O$]. The main economic hurdle for this technology is presumably that separation of the product stream would be energy-intensive.

The millisecond single-gauze reactor successfully couples catalytic and gas-phase chemistry to produce a highly unsta-

Correspondence concerning this article should be addressed to L. D. Schmidt.
Current address of R. P. O'Connor: Cargill Dow LLC, 15305 Minnetonka Blvd., Minnetonka, MN 55345.

ble, nonequilibrium species. A unique feature of the single-gauze chemical reactor is rapid preheat (on the order of 10^6 K/s), followed by fast thermal quenching to prevent decomposition of reactive intermediates. A portion of the cyclohexane feed reacts completely on the surface, generating heat and free radicals that initiate a gas-phase reaction sequence. The homogeneous chain reactions producing the desired oxygenated hydrocarbons and olefins are then thermally quenched by cold gases passing the wires.

The rates of homogeneous reactions of alkanes and oxygen are well established for fuel-lean processes, but there has been much less done for excess fuel with O_2 present. There currently is, to our knowledge, no detailed mechanism for cyclohexane partial oxidation in the literature. Existing hydrocarbon-oxidation models (Ranzi et al., 1997; Faravelli et al., 1998; Nehse et al., 1996; Chevalier et al., 1990) are well suited for total oxidation where fuel structure is relatively unimportant in determining the specific final products. While cyclohexane is a species in these mechanisms, its partial-oxidation products (cyclohexanone, 5-hexenal, etc.) are often lumped together, thereby rendering the models unsuitable for simulating fuel-rich experiments where high selectivities to specific species are observed.

In the last few years, faster computing resources and accurate descriptions of structure have rendered it practical and beneficial to rigorously model complex chemical processes using computational quantum chemistry. Density-functional theory (DFT) is a powerful computational technique that allows the calculation of the geometries and energetics of reactants, products, and transition-state intermediates in reactions (Labanowski and Andzelm, 1991; Kryachko and Ludeña, 1990; Chong, 1995). In this work, we have performed first-principles calculations using DFT to predict reaction enthalpies and elementary rate constants for the partial oxidation of cyclohexane.

In this article, reactor simulations are carried out using the density-functional kinetic mechanism. Four primary models are examined, in increasing order of rigor. The first calculation is for complete thermodynamic equilibrium of the system. Next, a one-dimensional (1-D) plug-flow model with the DFT gas-phase kinetic parameters is simulated. To include implicitly the thermal quenching in the wake region of the wires, a plug-flow reactor with a thermal history suggested by two-dimensional (2-D) inert-flow calculations is considered. In all these cases, wire temperatures must be assumed, and both surface chemistry and fluid dynamics are neglected.

The final model, and by far the most rigorous, incorporates 2-D flow around the catalytic wires. The 2-D model combines detailed computational fluid dynamics along with the density-functional elementary gas-phase reaction kinetics and mass-transfer-limited surface chemistry. A much better understanding of the experimental reactor is obtained from the 2-D simulations. In addition to simulating experiments, we can explore conditions that are not accessible in the experimental system—for example, higher reactor pressures. The model results are critically assessed and the limitations pointed out.

Gas-Phase Chemistry

Reactions modeled

The essential chemistry occurs strictly in the gas phase. This hypothesis is based on experimental evidence of reaction products (O'Connor and Schmidt, 2000a) as well as widely accepted alkane-oxidation schemes. Therefore, only the homogeneous reactions taking place after catalytic initiation are considered in the DFT calculations. The model includes 31 species and 46 reaction steps (23 elementary reactions all treated as reversible). Figure 1 sketches the important steps

Table 1. Reaction-Rate Parameters Calculated by Density-Functional Theory, Valid for 200–1,000°C.

Elementary Reaction	No.	A_f (mol, L, s)	$E_{a,f}$ (kcal/mol)	A_b (mol, L, s)	$E_{a,b}$ (kcal/mol)
$C_6H_{12} + O_2 \leftrightarrow C_6H_{11}\cdot + \cdot OOH$	1	2.72×10^{19}	54.1	4.38×10^{16}	0
$C_6H_{12} + \cdot OH \leftrightarrow C_6H_{11}\cdot + H_2O$	2	7.45×10^{20}	8.7	2.98×10^{18}	20.0
$C_6H_{12} \leftrightarrow C_6H_{11}\cdot + H\cdot$	3	1.93×10^{17}	103.3	1.23×10^{12}	1.4
$C_6H_{11}\cdot O_2 \leftrightarrow C_6H_{10} + \cdot OOH$	4	1.87×10^{16}	10.6	4.38×10^{16}	25.8
$C_6H_{11}\cdot O_2 \leftrightarrow C_6H_{11}OO\cdot$	5	4.38×10^{16}	0	9.02×10^{15}	30.4
$C_6H_{11}\cdot + \cdot OH \leftrightarrow C_6H_{11}OH$	6	1.01×10^{13}	1.2	1.44×10^{19}	87.8
$C_6H_{10} \leftrightarrow C_2H_4 + 1,3\text{-}C_4H_6$	7	1.56×10^{14}	75.3	1.89×10^{9}	40.6
$C_6H_{11}OO\cdot \leftrightarrow \alpha\text{-}C_6H_{10}OOH\cdot$	8	2.31×10^{11}	71.3	2.79×10^{8}	101.3
$C_6H_{11}OO\cdot \leftrightarrow \beta\text{-}C_6H_{10}OOH\cdot$	9	6.45×10^{15}	53.8	1.03×10^{16}	36.9
$C_6H_{11}OO\cdot \leftrightarrow \gamma\text{-}C_6H_{10}OOH\cdot$	10	5.63×10^{11}	27.2	4.63×10^{10}	9.8
$C_6H_{11}OO\cdot \leftrightarrow \delta\text{-}C_6H_{10}OOH\cdot$	11	4.31×10^{12}	75.6	2.79×10^{11}	58.1
$C_6H_{11}OO\cdot \leftrightarrow OC_6H_{11}O\cdot$	12	5.88×10^{14}	62.3	5.27×10^{11}	92.3
$\alpha\text{-}C_6H_{10}OOH\cdot \leftrightarrow (\alpha\cdot)\text{-}C_6H_{10}O\cdot + \cdot OH$	13	1.76×10^{19}	79.0	4.38×10^{16}	0
$\beta\text{-}C_6H_{10}OOH\cdot \leftrightarrow (\beta\cdot)\text{-}C_6H_{10}O\cdot + \cdot OH$	14	9.20×10^{22}	40.1	4.38×10^{16}	0
$\gamma\text{-}C_6H_{10}OOH\cdot \leftrightarrow (\gamma\cdot)\text{-}C_6H_{10}O\cdot + \cdot OH$	15	2.85×10^{21}	37.6	4.38×10^{16}	0
$\delta\text{-}C_6H_{10}OOH\cdot \leftrightarrow (\delta\cdot)\text{-}C_6H_{10}O\cdot + \cdot OH$	16	2.30×10^{21}	37.4	4.38×10^{16}	0
$OC_6H_{11}O\cdot \leftrightarrow C_5H_{10}O + \cdot CHO$	17	1.08×10^{10}	12.8	4.25×10^{4}	16.5
$\beta\text{-}C_6H_{10}OOH\cdot \leftrightarrow C_6H_{10} + \cdot OOH$	18	1.93×10^{14}	1.0	1.13×10^{5}	2.6
$(\alpha\cdot)\text{-}C_6H_{10}O\cdot \leftrightarrow c\text{-}C_6H_{10}O$	19	1.78×10^{13}	1.9	9.85×10^{13}	75.8
$(\beta\cdot)\text{-}C_6H_{10}O\cdot \leftrightarrow 1,2\text{-epoxy-}C_6H_{10}O$	20	1.82×10^{11}	6.5	9.11×10^{12}	58.8
$(\gamma\cdot)\text{-}C_6H_{10}O\cdot \leftrightarrow 1,3\text{-epoxy-}C_6H_{10}$	21	7.14×10^{11}	37.0	4.15×10^{14}	89.7
$(\gamma\cdot)\text{-}C_6H_{10}O\cdot \leftrightarrow 5\text{-}C_6H_{10}O$	22	9.43×10^{12}	0.2	2.63×10^{11}	59.2
$(\delta\cdot)\text{-}C_6H_{10}O\cdot \leftrightarrow 1,4\text{-epoxy-}C_6H_{10}O$	23	4.22×10^{11}	66.8	2.87×10^{11}	100.8

Note: The enthalpy of reaction is related to the activation energies by $\Delta H_R = E_{a,f} - E_{a,b}$.

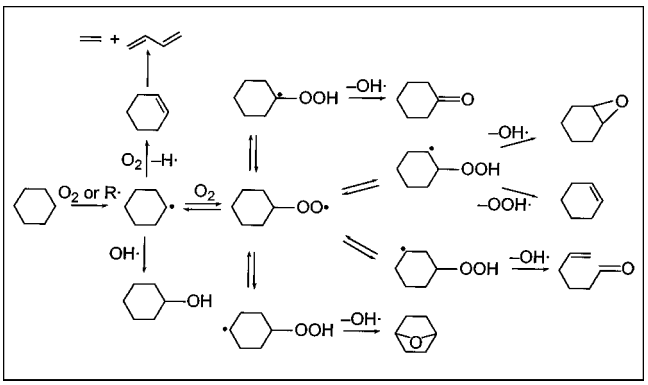

Figure 1. Suggested major pathways of fuel-rich cyclohexane partial oxidation.

Some intermediate steps included in the model have been omitted from the sketch, and all reactions are treated as reversible in the DFT mechanism.

in the mechanism, and Table 1 lists all reactions and DFT kinetic parameters.

The initial step in cyclohexane partial oxidation is almost certainly H-atom abstraction to form the cyclohexyl radical $C_6H_{11}\cdot$. These calculations consider an oxidative route

$$C_6H_{12} + O_2 \leftrightarrow C_6H_{11}\cdot + \cdot OOH$$

which forms a cyclohexyl and a hydroperoxy radical, as well as abstraction by a hydroxyl radical

$$C_6H_{12} + \cdot OH \leftrightarrow C_6H_{11}\cdot + H_2O$$

These initiation steps are compared to simple thermal C–H bond rupture

$$C_6H_{12} \leftrightarrow C_6H_{11}\cdot + H\cdot$$

in which oxygen is not required. The cyclohexyl radical can dehydrogenate oxidatively to form cyclohexene

$$C_6H_{11}\cdot + O_2 \leftrightarrow C_6H_{10} + \cdot OOH$$

or directly add an oxygen molecule to produce the important cyclohexylperoxy radical, $C_6H_{11}OO\cdot$:

$$C_6H_{11}\cdot + O_2 \leftrightarrow C_6H_{11}OO\cdot$$

Four primary pathways are hypothesized for the cyclohexylperoxy radical. It can rearrange by internal isomerization in which the peroxy radical bites back and abstracts an H atom, as in

$$C_6H_{11}OO\cdot \leftrightarrow \cdot C_6H_{10}OOH$$

There are four possibilities for this H-atom shift, since there are four unique carbon sites bearing hydrogen atoms:

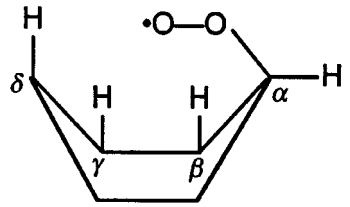

where the Greek letters refer to the specific H abstracted in $C_6H_{11}OO\cdot$ (α is the peroxy site). The cyclohexylperoxy radical prefers to undergo a backbiting abstraction of an internal H atom rather than the abstraction of an external one (Ranzi et al., 1997).

The cyclohexylperoxy isomers can lose hydroxyl radicals to produce diradical intermediates,

$$\cdot C_6H_{10}OOH \leftrightarrow \cdot C_6H_{10}O\cdot + \cdot OH$$

The diradical species are expected to quickly form products. The α-diradical forms cyclohexanone, β forms cyclohexene oxide, γ forms either 1,3-epoxy-cyclohexane or 5-hexenal, and δ forms 1,4-epoxy-cyclohexane. Cyclohexanone results from adjacent radicals forming a double bond. The epoxy-cyclohexanes are formed when a bond is created between two radicals. The γ-diradical can instead undergo C–C bond rupture to form an olefinic aldehyde, 5-hexenal. 5-Hexenal is experimentally significant, while 1,3-epoxy-cyclohexane is negligible, but so that the model is not biased *a priori*, both pathways are included in the model.

A channel involving a C–C $\alpha-\beta$ bond cleavage of the cyclohexylperoxy radical should be important (Zeelenberg and de Bruijn, 1965):

$$C_6H_{11}OO\cdot \leftrightarrow OC_6H_{11}O\cdot$$

where $OC_6H_{11}O\cdot$ is a linear aldehyde with an unpaired electron on the opposite oxygen. It can eject a formyl radical to form pentanal:

$$OC_6H_{11}O\cdot \leftrightarrow C_5H_{10}O + \cdot CHO$$

The C–OOH bond is β to the radical in the β-cyclohexylperoxy radical, so β-scission could be important, forming cyclohexene and a hydroperoxy radical:

$$\beta\text{-}C_6H_{10}OOH\cdot \leftrightarrow C_6H_{10} + \cdot OOH$$

At high temperatures, large amounts of ethylene and 1,3-butadiene are experimentally observed. The most likely route to these products is the decomposition of cyclohexene

$$C_6H_{10} \leftrightarrow C_2H_4 + 1{,}3\text{-}C_4H_6$$

which can be regarded as a double β-scission of a 1,2-cyclohexyl diradical (cyclohexene), with the reverse reaction being the Diels–Alder cycloaddition. We do not consider

other decomposition reactions that form minor products, such as acetaldehyde, and that would be more important at high temperatures.

Computational procedure for DFT calculations

All DFT calculations were performed with the Gaussian 98 software package (Gaussian, Inc., Rev. A.7, 2000) on a 200-MHz, 64-bit IBM SP Supercomputer. The geometry of the initial guess was optimized at the Hartree–Fock level of theory using the HF/6-21G method. The final geometry and thermodynamic calculations were done at the B3LYP/6-31+G(d) level of DFT theory. The B3LYP method uses Becke's three-parameter hybrid functional (Becke, 1988), which is a combination of the local exchange functional, the Hartree–Fock exchange, Becke's 1988 exchange functional correction, the gradient-corrected correlation functional of Lee, Yang, and Parr, and the local correlation functional of Vosko, Wilk, and Nusair. Diffuse functions, necessary to describe radicals in their excited states (Foresman and Frisch, 1996), were added to allow orbitals of heavy atoms to occupy a larger region of space. The B3LYP/6-31+G(d) method is spin-unrestricted, allowing open-shell electronic spin states, as required for free radicals.

Transition states were located by searching for a first-order saddle point on the potential-energy surface. The difference in energies between the reactants and the transition state corresponds to a reaction-rate constant according to transition-state theory

$$k = \frac{k_B T}{h} \frac{Q^{\ddagger}}{\prod_j Q_j} e^{-\Delta E_0^{\ddagger}/RT} = \frac{k_B T}{h} e^{-\Delta G^{\ddagger}/RT} \qquad (1)$$

where k_B is Boltzmann's constant, h is Planck's constant, $Q^{\ddagger}$ is the overall partition function of the transition state, Q_j is the partition function of reactant j, $\Delta E_0^{\ddagger}$ is the energy of activation, and $\Delta G^{\ddagger}$ is the free energy of activation. The Arrhenius activation energy, E_a, is related to the enthalpy of activation, $\Delta H^{\ddagger}$, by $E_a = \Delta H^{\ddagger} + RT$. The Arrehenius preexponential factor becomes $A = (ek_BT/h)e^{\Delta S^{\ddagger}/R}$, where $\Delta S^{\ddagger}$ is the entropy of activation.

DFT results

Table 1 summarizes the Arrenhius reaction-rate parameters for all reactions. These average values are valid over the range 200–1000°C. Over the range studied, activation energies typically varied by ~1 kcal/mol and preexponential factors varied by approximately a factor of 2. Because the error of this DFT method is expected to be at least ±3 kcal/mol, averages are appropriate. In a few cases where slightly negative activation energies (within the error of the technique) were predicted by the calculations, the elementary reactions were treated as barrierless with zero activation energies.

Reaction 1, which represents initiation by oxygen in the gas phase, was found to have a forward activation energy, $E_{a,f}$, of 54.1 kcal/mol. The activation energy of the reverse reaction, $E_{a,b}$, was 0, indicating that the combination of $C_6H_{11}\cdot$ and $\cdot OOH$ is a barrierless reaction. This result is consistent with known experimental and theoretical rates of radical–radical recombination reactions, which often have $E_a \approx 0$. The activation energy for initiation by a hydroxyl radical (reaction 2) was estimated as $E_{a,f} = 8.7$ kcal/mol. Also, the preexponential factor was over an order of magnitude higher for abstraction by $OH\cdot$. These initiation steps can be compared to C–H bond rupture (reaction 3), which was computed to have $E_{a,f} = 103.3$ kcal/mol.

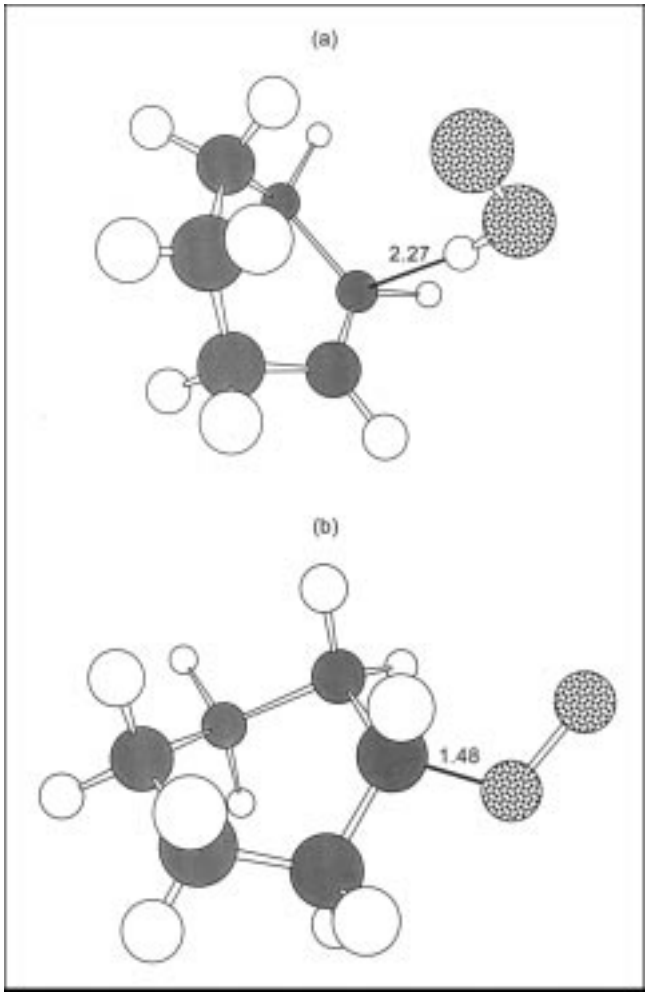

Figure 2. Transition states for reaction of $C_6H_{11}\cdot + O_2$ to (a) cyclohexene and $\cdot OOH$ in reaction 4 and to (b) $C_6H_{11}OO\cdot$ in reaction 5.

Numbers indicate bond lengths (in Å) in the transition-state complex.

The main competing pathways of $C_6H_{11}\cdot$ should be the formation of cyclohexene (reaction 4) vs. the cyclohexylperoxy radical (reaction 5). For reaction 4, $E_{a,f} = 10.6$ kcal/mol and $E_{a,b} = 25.8$ kcal/mol, while for reaction 5, $E_{a,f} = 0$ and $E_{a,b} = 30.4$ kcal/mol. Low temperatures should thus favor $C_6H_{11}OO\cdot$. Medium temperatures should promote the production of cyclohexene, and at high temperatures the decomposition of cyclohexene to ethylene and 1,3-butadiene (reaction 7, $E_{a,f} = 75.3$ kcal/mol) should be significant. Figure 2 compares the transition states for cyclohexene and cyclohexylperoxy-radical formation. Cyclohexene is formed when

oxygen abstracts an H atom adjacent to the radical site, while the cyclohexylperoxy radical results when O_2 simply adds to the radical site on $C_6H_{11}\cdot$.

Reactions 8 to 11 should be important sequences governing the oxygenate selectivities. Isomerization to the α-$C_6H_{10}OOH\cdot$ radical was found to be a high-barrier step, with $E_{a,f} = 71.3$ kcal/mol. This result is not surprising, considering the strain induced by the necessary four-membered ring in the transition state. Formation of β-, γ-, and δ-$C_6H_{10}OOH\cdot$ radicals had activation energies of $E_{a,f} = 53.8$, 27.2, and 75.6 kcal/mol, respectively. The most abstractable hydrogen should therefore be the γ-H atom, which is two carbon atoms away from the peroxy carbon. The transition state for the γ route includes a six-membered ring, which is known to be more stable than four-, five-, or seven-membered rings (as required for α, β, and δ, respectively). The bridge bond involved in the δ route causes a high activation energy for the formation of 1,4-epoxy-cyclohexane.

As a check on the accuracy of these DFT calculations, the enthalpy change of reaction 3 should equal the known C–H bond energy in cyclohexane. At 25°C, the bond strength is 97 kcal/mol (Weast, 1984), while $\Delta H_{298} = 100$ kcal/mol computed by DFT for reaction 3. A discrepancy of 3 kcal/mol is reasonable, as we do not regard these calculations to be more accurate than ± 3 kcal/mol. Computations at a higher level of theory (MP2) gave results consistent with the DFT kinetics. While the calculation of reaction enthalpies is straightforward, the estimation of rate parameters is highly sensitive to the quality of the transition-state structures, because small variations in activation energies correspond to large differences in rate constants.

Surface Chemistry

Although the products from the catalyst may be simple (such as CO, CO_2, and H_2O), the coupling of heterogeneous and homogeneous reactions can be quite complex. The fundamental problems with modeling the heterogeneous chemistry are that (1) rate expressions for most elementary steps are not known, (2) the role of surface structure must be neglected if rate expressions are to be developed, and (3) all parameters depend on coverages of all species on the surface. Surfaces also act as sinks and sources of free radicals that affect homogeneous-reaction steps. In excess hydrocarbon, mass transfer of oxygen likely controls the overall rate of the surface reactions (Dietz and Schmidt, 1995), because the sticking coefficients are near unity (Bharadwaj et al., 1996).

Bonding of cyclohexane to Pt occurs by C–H σ donation to the surface, which serves to weaken the C–H bonds (Kang and Anderson, 1985). At low temperatures and pressures, cyclohexane adsorbs on Pt at multiple bonding sites without C–C bond cleavage (Dietz et al., 1998). Upon adsorption, cyclohexane can begin to dehydrogenate. The initial removal of an H atom from adsorbed cyclohexane is the slowest step in the dehydrogenation (Kang and Anderson, 1985). With successive losses of H atoms, strong Pt–C bonds pull the C_6 skeleton even closer to the surface, and desorption becomes less favored. At low temperature and pressure where desorption rates are low, surface reactions can produce large amounts of benzene. For complete oxidation to CO and CO_2, carbon–carbon bonds obviously must be broken. The β-scission pathway forming ethylene and 1,3-butadiene also could be justified as a surface reaction, because βC–C bonds adjacent to an adsorbed C atom are weaker than the βC–H bonds. The endothermic ring opening could be driven by highly exothermic surface reactions.

For the 2-D reactor simulations the surface chemistry is modeled as

$$C_6H_{12} + \frac{15}{2}O_2 \rightarrow 3CO + 3CO_2 + 6H_2O$$

The assumption of equal proportions of CO and CO_2 is based on experimental data for a range of conditions over activated Pt–10%Rh catalysts (O'Connor and Schmidt, 2000a). The production of benzene and olefins by surface reactions is expected to be small (compared to CO_x) and is therefore neglected, based on prior work. Because mass transfer (of O_2) is assumed to control the rate of the surface reaction, specific kinetics are not necessary. Any cyclohexane and oxygen reaching the catalyst surface will instantly react, in the stoichiometric proportion indicated, to form CO_x, H_2O, and heat, which are transferred into the gas phase. Some of the heat also conducts into the gauze wire, the temperature of which is predicted by the 2-D model. Note that catalysts other than Pt–10%Rh can behave much differently than as suggested here (that is, the choice of catalyst is very important).

Equilibrium

We first examine the equilibrium distribution predicted by thermodynamics (HSC software) for a diluted mixture of cyclohexane and oxygen at various compositions and temperatures. Thermodynamics predict that for cyclohexane/oxygen ratios greater than the syngas ratio of 1/3, solid carbon is the major product at room-temperature equilibrium. For $C_6H_{12}/O_2 = 2.0$ with 30% nitrogen dilution at 25°C and 1.2 atm, the equilibrium composition is 46 mol % C(s), 33% CH_4, and 13% H_2O. As temperature increases, H_2 and CO_x become more significant, while CH_4 and H_2O decrease. Generally, for $C_6H_{12}/O_2 = 0.5$–5.0 and $T = 25$–825°C, no other species besides C(s), CO, CO_2, CH_4, H_2, H_2O, and N_2 exceed 0.1% at system equilibrium. Because solid carbon is not generally observed experimentally, calculations were performed where C(s) was not an allowable species. Without the possibility of coke deposition, benzene becomes a significant equilibrium species. As the temperature increases, syngas becomes more significant, overtaking benzene (but not methane) at > 800°C. A small amount ($\sim 0.3\%$) of ethylene is predicted at 800°C for these conditions. These calculations suggest that smaller olefins and (especially) benzene can be equilibrium products. However, the high experimental selectivities to cyclohexene (none predicted) and to oxygenates (identically zero at equilibrium) prove that this process cannot be described by thermodynamic equilibrium alone.

One-Dimensional Reactor Simulations

One-dimensional model

We must first simulate the nondispersive 1-D plug flow of an ideal-gas feed mixture. This model is a gross simplification of the actual process and is intended to be a sensitivity analy-

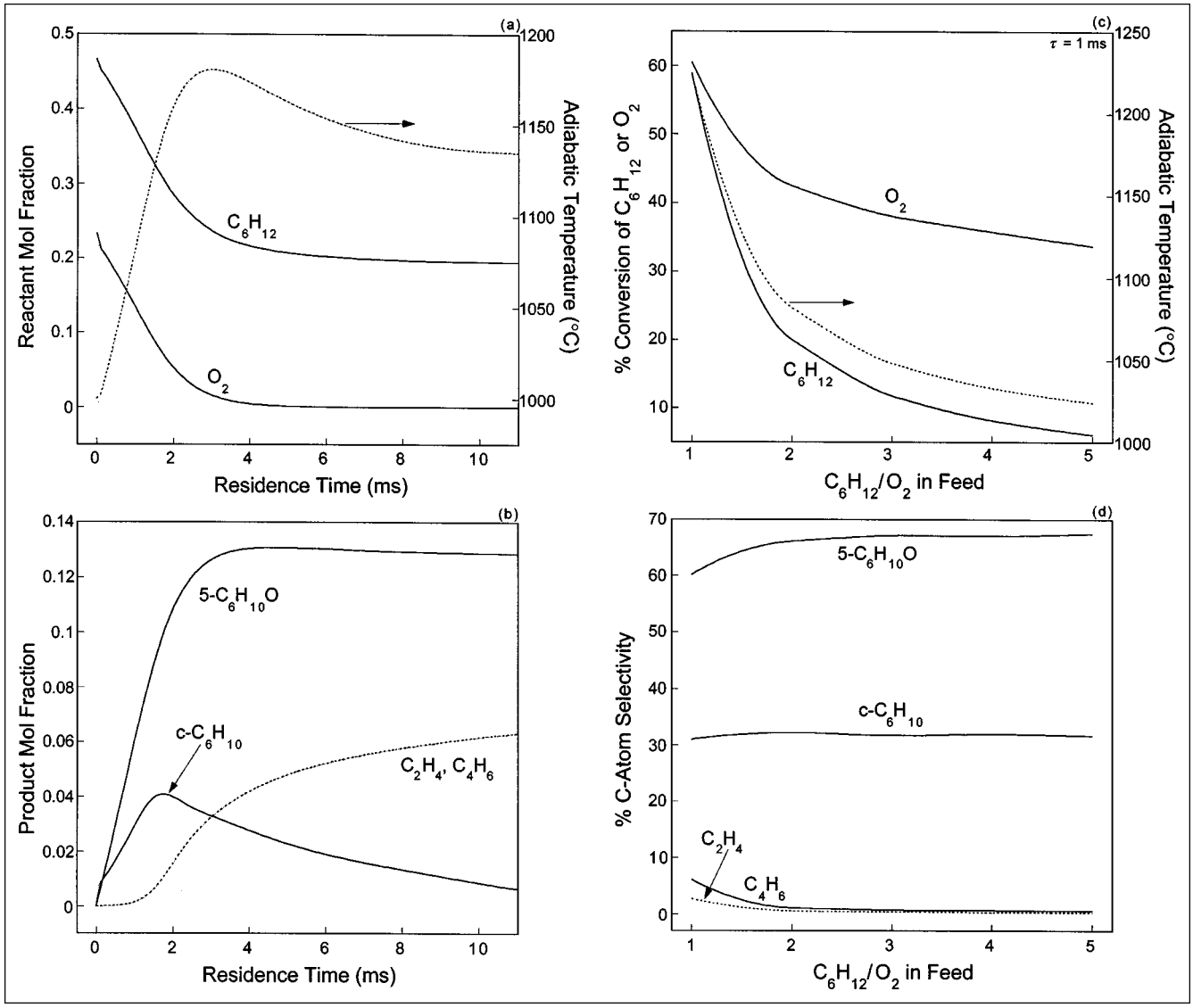

Figure 3. (a,b) Axial species and temperature for $C_6H_{12}/O_2 = 2$, $T_s = 1{,}000$°C (abiabatic), 30% N_2 dilution, $P = 1.2$ atm, and $u_0 = 0.194$ m/s; (c,d) effect of C_6H_{12}/O_2 for a reactor residence time of 1 ms.

sis of the proposed chemistry to the overall rate and product selectivities. The Chemkin 3.6 software package (Reaction Design, 1999) is used along with the program PLUG (Larson, 1996). PLUG solves the set of differential equations describing the reactor using the implicit numerical solver DASSL (Petzold, 1982). The input here consists of reaction kinetic parameters (for 46 reactions), thermodynamic data (heat capacity, enthalpy, and entropy as polynomial fits in temperature) for all 31 species from the DFT calculations, and the inlet conditions for the reactor. Calculations were not CPU-intensive, requiring ~ 1 minute on a desktop computer.

In these simulations, we use the catalyst temperature, T_s, as the entrance temperature ($z = 0$) to a homogeneous plug-flow reactor. The experimental catalyst temperature is extremely difficult to measure. It is not possible to measure T_s with a thermocouple, because the thermocouple wire becomes catalytically active and reports a fictitious temperature (as well as disrupting the flow field near the wire). By pyrometer, the catalyst has been estimated to be 900 ± 100°C for a gas-phase temperature of ~ 500°C measured 5 mm downstream (by a thermocouple in a thermowell). Lower and upper bounds of $T_s = 800$°C and 1000°C were considered in the 1-D approach. The 2-D model below, which includes surface chemistry, can predict a value of T_s.

Results for the one-dimensional model

For base-case conditions ($C_6H_{12}/O_2 = 2$, 30% N_2 dilution, reactor pressure $P = 1.2$ atm, and inlet velocity $u_0 = 0.194$ m/s) and an entrance temperature, $T_s = 800$°C, a long residence time (> 25 ms) was required for the chemistry to be completed (results not shown). The major oxygenate and olefin were the same as those observed experimentally: 5-hexenal and cyclohexene. For $\tau > 1$ ms, 5-hexenal was by far

the most significant product, according to the model. The initial selectivities to 5-hexenal and cyclohexene were approximately equal at $\tau \approx 0.5$ ms, but the conversions were minimal at this residence time. The minor products, in order of decreasing concentration, were cyclohexene oxide > pentanal > cyclohexanone > cyclohexanol > 1,3-epoxy-cyclohexane > 1,4-epoxy-cyclohexane. All of these species were predicted in amounts at least an order of magnitude less than 5-hexenal.

Figures 3a and 3b show axial temperature and species profiles for base-case conditions and $T_s = 1000$°C. With an entrance temperature of 1000°C, most of the conversion of C_6H_{12} and O_2 happened in the first three milliseconds. The maximum temperature (~ 1175°C) also occurred at $\tau \approx 3$ ms, which would be upstream of the location of the thermocouple (25 ms). 5-Hexenal still dominated the product distribution, but cyclohexene was relatively more important for $T_s =$ 1000°C compared to 800°C. Decomposition of C_6H_{10} to C_2H_4 and C_4H_6 was significant for the higher temperature. Figures 3c and 3d show the effect of the cyclohexane/oxygen ratio for $T_s = 1000$°C and $\tau = 1$ ms. The specific selectivity to cyclohexene ($\sim 30\%$) was correct, but the selectivity to 5-hexenal ($> 60\%$) was much higher than that observed ($\sim 25\%$). This result suggests that decomposition routes of 5-hexenal may be important. While selectivities were not in agreement, the same trends in cyclohexane conversion and temperature were observed experimentally.

Plug flow with a prescribed temperature profile

The plug-flow model assumed that the gas is uniformly heated to the catalyst temperature, when in fact the large spacing between adjacent wires in the 40-mesh gauze means that radial variations must be important. Two-dimensional computational fluid-dynamic calculations of flow normal to infinite cylinders, heated isothermally to T_s, were performed for nonreacting flows, but with the correct reactants, properties, and fluid dynamics. From these 2-D calculations, the axial temperature profile $T(z)$ along the line of symmetry normal to the wire is prespecified along the length of a 1-D plug-flow reactor. This model is now "pseudo−two-dimensional" (P−2-D).

Simulations were performed for the base-case conditions with the lower and upper bounds for the wire, $T_s = 800$°C and 1,000°C, and for cyclohexane/oxygen ratios from 1 to 5. Figure 4a summarizes the results for $T_s = 1{,}000$°C, showing the axial profiles of reactant mole fractions along with the imposed temperature profile. The gas temperature, initially at $T_0 = 200$°C, rose $> 10^5$ K/s and attained an assumed surface temperature of 1000°C. The upstream edge of the wire is situated at $\tau = 0$. The reactant-depletion zone was necessarily confined to a few milliseconds, because the specified temperature rapidly quenched to the point of shutting off the chemistry. The conversions of cyclohexane and oxygen were 23% and 45%, respectively. 5-Hexenal was substantially favored (77% selectivity) compared to cyclohexene (22% selectivity).

The model predicts the *gas-phase* conversion. If all the experimental CO_x is a surface-only product, then it is possible to determine the surface conversions of reactants and add them to the gas-phase conversions calculated by the simulation. At the base case of $C_6H_{12}/O_2 = 2$, the effective (surface plus gas-phase) conversions of C_6H_{12} and O_2 became 27%

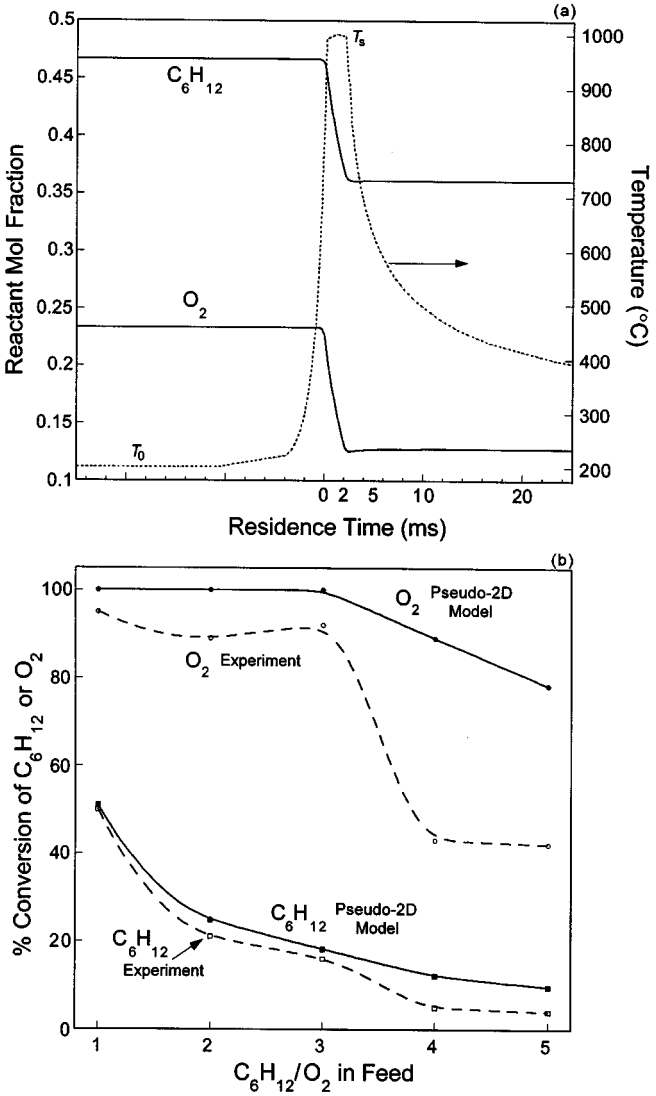

Figure 4. (a) Reactor species profiles with a prescribed 2-D temperature for $C_6H_{12}/O_2 = 2$, $T_s =$ 1,000°C, 30% N_2, $P = 1.2$ atm, and $u_0 = 0.194$ m/s; (b) conversions predicted by the P−2-D model vs. experiment, where all CO_x is assumed to originate from surface reactions.

and 100%, respectively (Figure 4b), while the selectivities were as follows: 62% to 5-$C_6H_{10}O$, 18% to C_6H_{10}, 10% to CO, and 10% to CO_2. For $T_s = 800$°C, limited conversions (3% of C_6H_{12} and 7% of O_2) were attained, suggesting that the actual surface temperature for $C_6H_{12}/O_2 = 2$ was probably closer to 1000°C in order to account for the experimental conversions—unless considerable surface-radical generation speeds up the chemistry. Figure 4b compares these conversions predicted by the P−2-D model to experimental data for the single-gauze reactor. The trends are correct, especially for cyclohexane, but the oxygen conversion was significantly overpredicted and the sharp drop-off for $C_6H_{12}/O_2 > 3$ was not captured. Selectivity trends, not shown, were similar to 1-D results, with 5-$C_6H_{10}O$ the major product at all condi-

tions. Therefore, the P−2-D model also failed to quantitatively describe the experimental selectivities to the major C_6 products.

Discussion and limitations of the plug-flow models

The DFT mechanism was used to perform one-dimensional plug-flow simulations of the single-gauze reactor. Profiles of both species and temperature along the length of the reactor for entrance temperatures of 800°C and 1,000°C showed that (1) the reaction times necessary were realistic, especially for $T_s = 1{,}000$°C; (2) the dominant products were 5-hexenal and cyclohexene, with 5-hexenal significantly overpredicted; and (3) decomposition of cyclohexene to ethylene and 1,3-butadiene was important at high temperatures.

A direct comparison of the 1-D model along with the experiment is in fact difficult because the model completely ignores radial variations in temperature as well as downstream heat losses. The products in the real reactor are withdrawn at a location corresponding to τ of hundreds (or even thousands) of milliseconds. The model assumes a radially uniform T_s and the absence of heat losses, which are experimentally important far downstream of the catalyst. The rapid decrease in temperature downstream of the single-gauze wires causes the reaction zone to be smaller than predicted by the 1-D calculations. It is the nonuniform nature of the temperature profile that is presumably allowing the preservation of unstable species. Pure plug flow, with a uniform gas composition and temperature, is precisely what is *not* happening in the reactor.

A (pseudo−2-D) model was able to describe conversions reasonably well. By artificially summing up predicted gas-phase conversions with experimentally determined surface conversions, qualitative agreement was obtained. While promising, there unfortunately was no improvement in the prediction of selectivities to major products in the P−2-D simulation, as compared to the 1-D model. The P−2-D approximation, while useful in mimicking the quenching effect, ultimately fails to be a robust model. Plug flow cannot account for back-diffusion of radicals (which can decrease the required residence times for a given conversion). The narrow reaction zone causes extremely large gradients in temperature, concentrations, and properties near the catalyst, and these variations cannot be described by plug flow with constant properties and uniform temperature. The thermal quenching in the gauze wake is the major unresolved issue. Rigorous numerical simulations applying the correct geometry, equations, and properties for the transport of mass, heat, and momentum are necessary to provide axial and radial temperature and concentration profiles of all species. A complete calculation should combine surface and gas-phase chemistry with species diffusion and heat transfer in flow normal to cylindrical wires.

Two-Dimensional Reactor Simulations

Two-dimensional model

The conservation of mass in 2-D Cartesian coordinates (x and y) is

$$\frac{\partial \rho}{\partial t} + \frac{\partial}{\partial x}(\rho u_x) + \frac{\partial}{\partial y}(\rho u_y) = 0 \tag{2}$$

where ρ is the density and u_x and u_y are the components of the velocity vector $\boldsymbol{u}$. The continuity equation is coupled with the conservation of momentum, which has two components (x and y)

$$\frac{\partial}{\partial t}(\rho u_x) + \frac{\partial}{\partial x}(\rho u_x u_x) + \frac{\partial}{\partial y}(\rho u_x u_y) = -\frac{\partial P}{\partial x} + \frac{\partial \tau_{xx}}{\partial x} + \frac{\partial \tau_{xy}}{\partial y} \tag{3}$$

$$\frac{\partial}{\partial t}(\rho u_y) + \frac{\partial}{\partial y}(\rho u_y u_y) + \frac{\partial}{\partial x}(\rho u_y u_x) = -\frac{\partial P}{\partial y} + \frac{\partial \tau_{yy}}{\partial y} + \frac{\partial \tau_{yx}}{\partial x} \tag{4}$$

where gravity effects are neglected. Here P is the static pressure, and the viscous stress tensors are given by

$$\tau_{xx} = 2\eta \frac{\partial u_x}{\partial x} - \frac{2}{3}\eta\left(\frac{\partial u_x}{\partial x} + \frac{\partial u_y}{\partial y}\right) \tag{5}$$

$$\tau_{xy} = \eta\left(\frac{\partial u_x}{\partial y} + \frac{\partial u_y}{\partial x}\right) \tag{6}$$

Density in this model is computed from the ideal-gas law as

$$\rho = \frac{P}{RT\sum(m_j/M_j)}, \tag{7}$$

where m_j is the mass fraction and M_j the molecular weight of species j. The conservation of species j is described by

$$\frac{\partial}{\partial t}(\rho m_j) + \frac{\partial}{\partial x}(\rho u_x m_j) + \frac{\partial}{\partial y}(\rho u_y m_j) = \frac{\partial J_{j,x}}{\partial x} + \frac{\partial J_{j,y}}{\partial y} + S_j \tag{8}$$

where $J_{j,i}$ is the diffuse mass flux of species j in the ith direction and S_j is the net rate of production of species j per unit volume due to chemical reaction. The calculation of the species concentrations at the catalyst surface is based on a balance of the convection and diffusion of each species to/or from the surface and the rate at which it is consumed or produced at the surface. This flux balance for species j is

$$(\rho \boldsymbol{v} m_j + \boldsymbol{J}_j) \cdot \boldsymbol{n} = R_j'' \tag{9}$$

where $\boldsymbol{v}$ is the bulk velocity at the surface, $\boldsymbol{n}$ is the unit normal vector to the surface, and R_j'' is the rate of surface reaction (per unit area) of species j.

The conservation of energy, in terms of static enthalpy H, is

$$\frac{\partial}{\partial t}(\rho H)+\frac{\partial}{\partial x}(\rho u_x H)+\frac{\partial}{\partial y}(\rho u_y H) = \frac{\partial}{\partial x}\left(k\frac{\partial T}{\partial x}\right)+\frac{\partial}{\partial y}\left(k\frac{\partial T}{\partial y}\right)-\frac{\partial}{\partial x}\sum H_j J_j - \frac{\partial}{\partial y}\sum H_j J_j+\frac{\partial P}{\partial t}+u_x\frac{\partial P}{\partial x}+u_y\frac{\partial P}{\partial y}+S_H \quad (10)$$

where k is the mixture thermal conductivity and S_H is a source term due to chemical reaction:

$$S_H=\sum_j H^o_{f,j}R_j \quad (11)$$

where R_s the net rate of reaction for species j summed over all reactions (index i)

$$R_j=\sum_i R_{j,i} \quad (12)$$

In the conducting solid catalyst wire, the conduction equation

$$\frac{\partial}{\partial t}(\rho_w H_w)=\frac{\partial}{\partial x}\left(k_w\frac{\partial T}{\partial x}\right)+\frac{\partial}{\partial y}\left(k_w\frac{\partial T}{\partial y}\right) \quad (13)$$

is solved simultaneously with the enthalpy transport equation (Eq. 10) to yield coupled conductive/convective heat transfer. The heat release by the exothermic surface reactions not only heats up the gases flowing near the catalyst but also heats up the catalyst itself, since it is modeled as a conducting wall. In Eq. 13, ρ_w is the density of Pt−10%Rh, taken to be 2055 kg/cm^3; H_w is the wall enthalpy, $C_w(T-T_{\text{ref}})$, where C_w = 228.1 J/kg·K, the heat capacity of Pt−10%Rh; and k_w is the catalyst thermal conductivity, 83.4 W/m·K. All catalyst properties are assumed constant and equal to mass-averaged properties of pure Pt and Rh.

The specific heat capacity of each component is calculated from a three-coefficient polynomial in temperature adapted from the DFT calculations. The composition-dependent heat capacity of the mixture is then computed as a mass-fraction-weighted average:

$$C_p=\sum_j m_j C_{p,j} \quad (14)$$

Viscosities of individual components are calculated by kinetic theory:

$$\eta_j=2.67\times10^{-6}\frac{\sqrt{M_j T}}{\sigma_j^2\Omega_\eta} \quad (15)$$

where Ω_η is a reduced collision integral, a function of σ and ϵ/k, the Lennard−Jones size and potential-energy parameters, respectively. They are taken from Welty et al. (1984), Fluent (1998), or estimated by analogy. The mixture viscosity is a composition-dependent, mol-fraction-weighted viscosity. Thermal conductivities of individual components are computed via kinetic theory as

$$k_j=\frac{15}{4}\frac{R}{M_j}\eta_j\left(\frac{4}{15}\frac{C_{p,j}M_j}{R}+\frac{1}{3}\right) \quad (16)$$

and a composition-dependent mixture thermal conductivity is calculated at each iteration. The diffusivity of species j in the mixture, $D_{j,\text{mix}}$ is computed from

$$D_{j,\text{mix}}=\frac{1-X_j}{\sum_{j,k\neq j}X_j/D_{jk}} \quad (17)$$

where X_j is the mol fraction of species j and D_{jk} is the binary mass-diffusion coefficient for species j in species k. The binary diffusion coefficients are also calculated by kinetic theory:

$$D_{jk}=0.0188\frac{\left[T^3\left(\frac{1}{M_j}+\frac{1}{M_k}\right)\right]^{1/2}}{P\sigma_{jk}^2\Omega_D} \quad (18)$$

where Ω_D is another collision integral.

Chemistry

Because of the computational demands for this problem, it is beneficial to exclude from the mechanism those reactions and species that are observed by the 1-D calculations to be of minimal importance. The insignificant reactions were deemed to be thermal initiation of cyclohexane and the reactions involving 1,3-epoxy-cyclohexane, 1,4-epoxy-cyclohexane, and cyclohexanol. These three product species, along with hydrogen and the δ-cycloperoxy radical and diradical, are therefore removed from the mechanism.

The surface chemistry is modeled as

$$C_6H_{12}+\frac{15}{2}O_2\rightarrow 3CO+3CO_2+6H_2O$$

where the rate of this reaction is mass-transfer limited. The surface kinetics are specified such that the reaction rate is fast and insensitive to the kinetic parameters assumed because of mass-transfer control. Overall, the 2-D model includes 25 species and 35 reactions (34 elementary gas-phase reactions and one lumped surface step). The possible stable products are cyclohexene, ethylene, 1,3-butadiene, 5-hexenal, cyclohexanone, cyclohexene oxide, pentanal, carbon monoxide, carbon dioxide, water, and unreacted cyclohexane and oxygen (along with nitrogen diluent).

Computational procedure

To solve the transport equations in the appropriate geometry, we used Fluent (Version 4.5.2, 1998), a state-of-the-art computational fluid-dynamics (CFD) software package de-

signed to model detailed flow physics, including reactions. The geometry was that of infinite cylindrical wires separated by a distance equivalent to the 40-mesh single-gauze wire spacing, or about five wire diameters. The single-gauze wire diameter was taken to be 100 μm, consistent with experimental measurements after catalyst activation, so the spacing was ~ 500 μm. While computational grids should be highly resolved for accuracy, there must be a trade-off with computation time, especially when chemistry is involved. The grid developed for these 2-D simulations employs 1274 cells, with the region near the wire more finely resolved. There are two planes of symmetry—one through the middle of a wire, and one midway between adjacent gauze wires. Distances equivalent to approximately three wire diameters upstream and five downstream were included in the grid. For a superficial velocity of 0.194 m/s (base case), the grid encompassed approximately five milliseconds axially in residence time.

Inlet conditions were the feed temperature ($T_0 = 200$°C), the velocity ($u_x = 0.194$ m/s, $u_y = 0$), the mol fractions of the feed mixture (usually 0.466 for C_6H_{12}, 0.233 for O_2, and 0.300 for N_2), and the pressure (typically 1.2 atm). Boundary conditions included zero flux of all quantities across symmetry lines, no slip at the wall, and zero-flux surface-boundary conditions for all species except those participating in surface reactions. The solution procedure chosen for these simulations was second-order-upwind, finite-difference integration of the transport equations. Fluent uses an iterative scheme, with integration implicit in time.

Solution was difficult for a number of reasons. First, the impact of the reactions on the basic flow pattern is strong, leading to strong coupling between the mass/momentum balance and the species transport equations. Large gradients in properties that vary with composition and temperature also caused convergence problems. Finally, the chemistry was extremely stiff, meaning that some reaction rates were much more rapid than convection and diffusion rates. Because the flow field was highly coupled with the temperature field, the transport equations were underrelaxed. During iterations, new values were updated to only a fraction (the underrelaxation factor) of the calculated value. Generally, in these simulations, initial underrelaxation factors (especially enthalpy) needed to be ≤ 0.1 to avoid divergence. Toward the end of the solution process, these factors were increased to 0.5 or greater to speed up convergence.

A sequential approach was also used to aid convergence. The first step was to solve the temperature profile for flow of the 30%-diluted cyclohexane/oxygen mixture over a hot wire but without chemistry. This calculation was straightforward and was the basis for the temperature profile in the P–2-D model. Then, surface chemistry was enabled so that combustion on the wire supplied the heat. The flow needed to be "numerically ignited" with a hot (isothermal) surface. Next, the initiation reactions for the gas-phase chemistry were turned on. Finally, all 35 reactions were enabled, with the surface temperature determined by the chemistry, conduction, and convection involving the catalytic wire. At each iteration, $\sim 35{,}000$ calculations were performed in the grid, and therefore on the order of 10 billion total calculations were necessary to solve this problem. The final solution for the base case required $> 200{,}000$ iterations overall and $\sim 1{,}000$ single CPU hours on an IBM SP Supercomputer.

Two-dimensional simulation of base case

Figures 5 and 6 summarize results for the base case of $C_6H_{12}O_2 = 2$, 30% N_2, $T_0 = 200$°C, $P = 1.2$, atm, $u_0 = 0.194$ m/s. Figure 5 shows contours of temperature. The flow entered at 200°C, reached a catalyst temperature (calculated) of 919°C, and under adiabatic conditions fell to 536°C far downstream from the catalyst where the flow becomes uniform. Gases passing near the wire heated up significantly while cold gases between the wires rapidly cooled these hot gases. Immediately upstream of the catalyst, the gradient in temperature was 5.2×10^6 K/m and 6.3×10^5 K/s. This rapid heating of the gases was followed by fast thermal quenching in the wake of the wire, where the gradient in temperature was -2.0×10^6 K/m and -2.4×10^5 K/s. Similar gradients were present in gas properties because they vary with temperature (and concentrations).

Figures 6a and 6b show contours of reactants cyclohexane and oxygen. The cyclohexane mole fraction was initially 0.466, fell to a minimum value of 0.326 at the surface, and became 0.36 at the exit. This mol fraction corresponds to a C_6H_{12} conversion of 16.8%. The oxygen mol fraction, 0.233 in the feed, decreased to zero at the surface because of its rapid depletion in the surface reaction. The absence of O_2 near the catalyst wire is consistent with the assumed mass-transfer-controlled surface chemistry. The final mol fraction of oxygen was 0.05, and the O_2 conversion was 77.5%. The con-

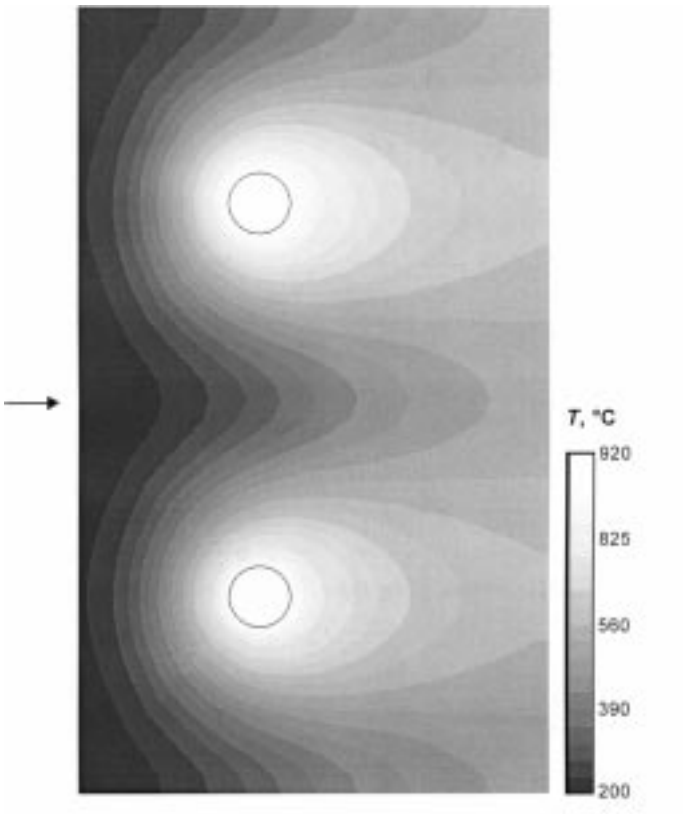

Figure 5. Contours of temperature in and around the catalytic wire, predicted to be at a temperature $T_s \approx 920$°C

$C_6H_{12}/O_2 = 2$, 30% N_2, $T_0 = 200$°C, $P = 1.2$ atm, and $u_0 = 0.194$ m/s.

versions of both reactants were underpredicted compared to experiment (Table 2). Although the concentration of reactants dropped very quickly upon entering the grid region, there was not actually any conversion until very near the catalyst. The upstream decrease in mol fractions was due solely to species diffusion.

Figures 6c and 6d show the contour plots of the major products cyclohexene and 5-hexenal. Cyclohexene was maximized near the catalyst, both up- and downstream, at a mol fraction of 0.05. 5-Hexenal, on the other hand, was maximized in the wake of the wire (also at ~ 0.05 mol fraction). Because of differences in rates of reverse reactions, cyclohexene decomposition to ethylene and butadiene, and a larger zone of 5-hexenal formation, the final mol fraction of 5-hexenal was 0.035, while that of cyclohexene was 0.025. The C-atom selectivities to these products were 42% to 5-$C_6H_{10}O$ and 30% to C_6H_{10}. Although the concentration of 5-hexenal does not become uniform, the formation rates for all species have dropped to zero at the exit of the grid region, according to the simulation. In fact, the formation zone of these primary products was relatively small (< 1 ms in residence time). Downstream of the grid exit, there is of course species diffusion, but the overall mol fractions should remain at the average values predicted at the exit. Table 2 compares experimental and predicted temperatures, conversions, and selectivities, while Table 3 compares the mol fractions measured by gas chromatography to those calculated by the 2-D model.

In general, low temperatures should favor the cyclohexylperoxy radical, while at high temperatures, $C_6H_{11}OO\cdot$ is expected to decompose back to $C_6H_{11}\cdot$ and O_2 (Ranzi et al., 1997; Nehse et al., 1996). The equilibrium between $C_6H_{11}\cdot$ and $C_6H_{11}OO\cdot$ is anticipated to be rapid. Near the catalyst, the calculated rate of the reverse reaction ($C_6H_{11}OO\cdot \rightarrow C_6H_{11}\cdot + O_2$) was significant and there was no $C_6H_{11}OO\cdot$ present. On the other hand, $C_6H_{11}\cdot$ was at its highest concentration very near the surface. The cyclohexyl concentration was zero in most of the computational grid (except near the wire) and its maximum mol fraction was an order of magnitude smaller than that of the cyclohexylperoxy radical.

Predicted trends with C_6H_{12}/O_2 ratio

Starting with the converged simulations highlighted in the previous section, the operating conditions were modified to consider different cyclohexane/oxygen feed ratios. Figure 7 summarizes the results for $C_6H_{12}/O_2 = 1$, 2, and 4. Contour plots are qualitatively similar to the base-case figures and will not be shown.

The surface temperature was predicted to be 1081°C for $C_6H_{12}/O_2 = 1$. The adiabatic temperature (642°C) compares reasonably well to the experimental measurement (~ 575°C) 5 mm downstream. The conversions were again underpredicted: 37% vs. 50% experimentally for C_6H_{12}, and 86% vs.

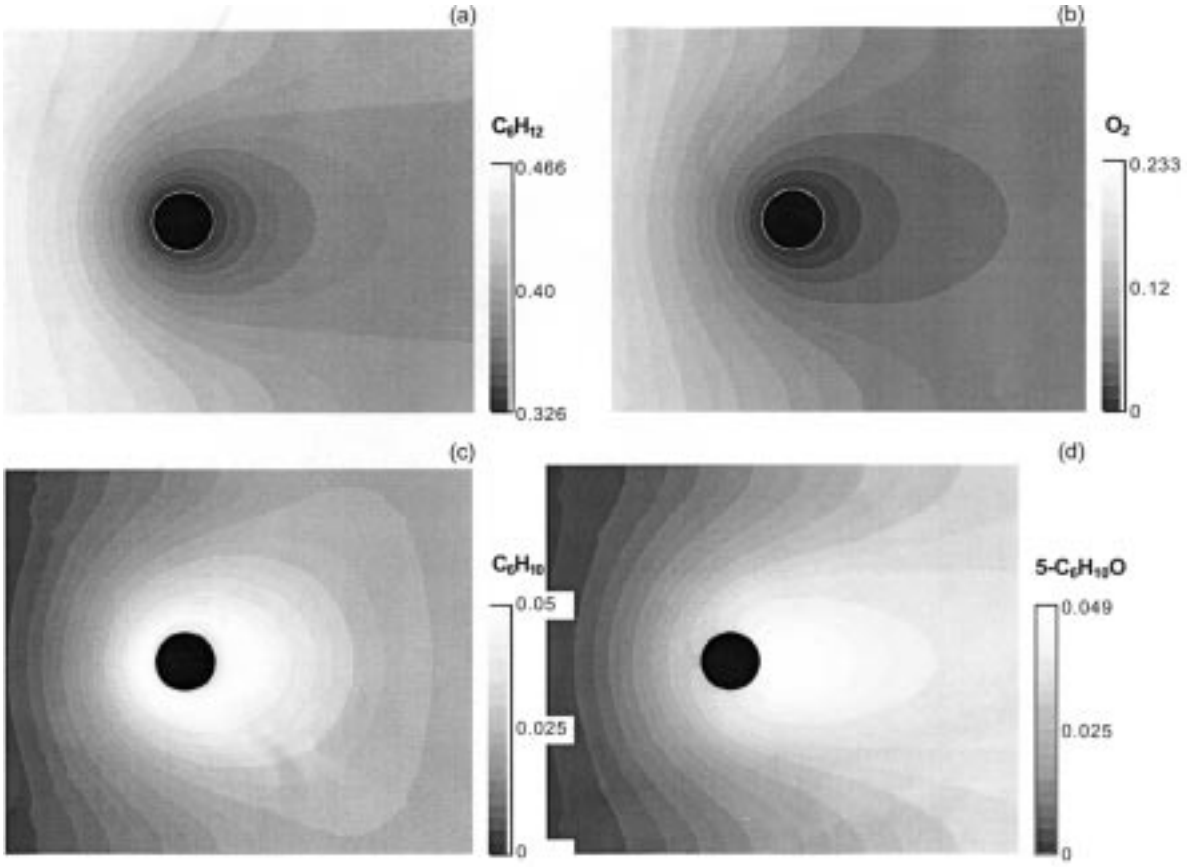

Figure 6. Contours of (a) cyclohexane, (b) oxygen, (c) cyclohexene, and (d) 5-hexenal mol fractions.

Table 2 lists the predicted conversions and selectivities. $C_6H_{12}/O_2 = 2$, 30% N_2, $T_0 = 200$°C, $P = 1.2$ atm, and $u_0 = 0.194$ m/s.

Table 2. 2-D Model vs. Experimental Results for 40-mesh Pt–10%Rh

	Experiment	2-D Model
Surface Temperature	~ 850°C (pyrometer)	919°C
5-mm Temperature	476°C (thermocouple)	536°C (adiabatic)
Conversion of C_6H_{12}	25.0	16.8
Conversion of O_2	89.5	77.5
Oxygenate Selectivity	42.9	42.1
Olefin Selectivity	38.8	35.9
CO_x Selectivity	18.0	22.0
C_6H_{10} Selectivity	31.3	30.0
5-$C_6H_{10}O$ Selectivity	25.0	41.9
$C_5H_{10}O$ Selectivity	10.3	< 0.1
c-$C_6H_{10}O$ Selectivity	0.1	0.6
C_2H_4 Selectivity	1.8	2.0
CO Selectivity	8.9	11.0
CO_2 Selectivity	9.1	11.0
C_6H_6 Selectivity	4.5	—

Note: $C_6H_{12}/O_2 = 2$; 30% N_2; 2.5 SLPM or $u_0 = 0.194$ m/s; $T_0 = 200$°C; and $P = 1.2$ atm.

95% for O_2 (Figure 7a) The simulation for $C_6H_{12}/O_2 = 1$ calculated too much 5-hexenal and CO_x, but the olefins agreed very well. Namely, the cyclohexene selectivity was 14% vs. 15% experimentally, and its decomposition products totaled 27% vs. 30% selectivity in the laboratory (Figure 7b). For $C_6H_{12}/O_2 = 4$, the adiabatic temperature was 432°C, which again was reasonable (~ 375°C experimentally). According to the model, the actual reactor is close to (but not entirely) adiabatic. The conversions of C_6H_{12} and O_2 dropped to 8% and 53%, respectively, compared to 5% and 42% for the $C_6H_{12}/O_2 = 4$ experiment. For this feed ratio, the computed selectivity to 5-hexenal (27%) was close to the data (25%), whereas cyclohexene was now somewhat overpredicted (44% vs. 30% experimentally).

Predicted trends with reactor pressure

Figure 8 summarizes results for different simulated reactor pressures: 1.2, 2, and 10 atm (121.6, 202.7, and 1013 kPa). The inlet mass flow is raised as the pressure is increased so the superficial catalyst contact time is maintained at 0.7 ms. Contour plots for 2 and 10 atm were qualitatively similar to

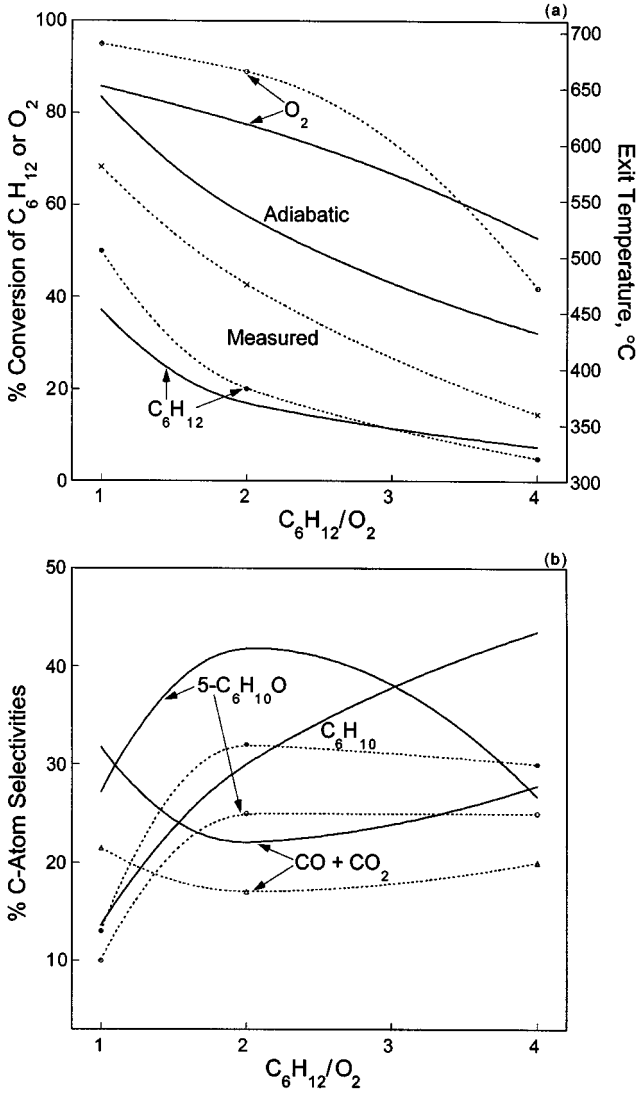

Figure 7. 2-D simulation vs. experiment for varying C_6H_{12}/O_2 ratio ($T_0 = 200$°C, 30% N_2, $P = 1.2$ atm, and $u_0 = 0.194$ m/s).

Solid lines are model predictions, and dashed lines are experimental trends.

Table 3. Species mol fractions in 2-D Model vs. Experimental Results for 40-mesh Pt–10%Rh

Species	Experiment	2-D Model
N_2	0.277	0.278
C_6H_{12}	0.323	0.360
O_2	0.025	0.049
CO	0.055	0.054
CO_2	0.055	0.056
H_2O	0.161	0.130
C_6H_{10}	0.034	0.025
5-$C_6H_{10}O$	0.027	0.035
1.2-$C_6H_{10}O$	0.0001	0.00005
c-$C_6H_{10}O$	0.0007	0.0001
C_2H_4	0.006	0.005
C_4H_6	0.002	0.005
$C_6H_{10}O$	0.013	0

Note: $C_6H_{12}/O_2 = 2$; 30% N_2; 2.5 SLPM or $u_0 = 0.194$ m/s; $T_0 = 200$°C; and $P = 1.2$ atm.

the base-case plots. The 10-atm profiles tend to be pushed downstream (due to the higher gas velocity). At $P = 2$ atm, the adiabatic temperature was found to be 550°C, which again was somewhat above the 5-mm measured value of 495°C. From Figure 8a, the conversion of C_6H_{12} was low by four percentage points, and O_2 conversion was significantly low at 81% (no breakthrough of O_2 was observed experimentally at 2 atm). The 2-atm simulation predicted too much 5-hexenal and not enough cyclohexene, compared to the experiment (Figure 8b). One reason is that more decomposition of cyclohexene occurred in the simulation. Cyclohexene oxide, which was barely detectable in the experiments, was at 9% selectivity for the 2-atm calculation. The simulated trend in CO + CO_2 formation between 1.2 and 2 atm was qualitatively correct, but the model did not predict the extent of the falloff in CO_x formation at higher pressure.

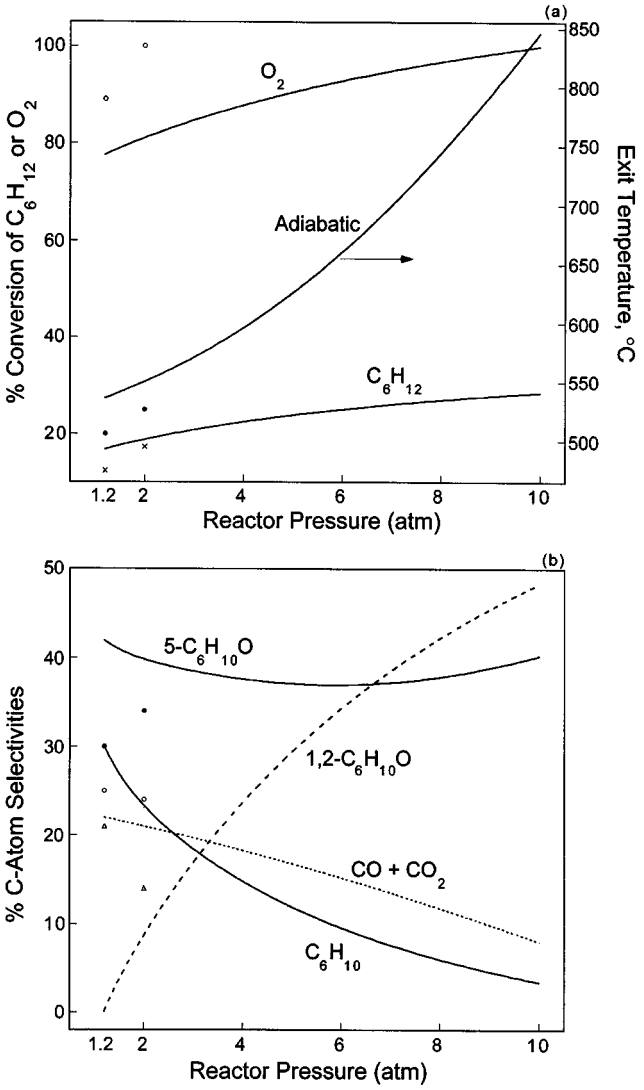

Figure 8. Prediction of 2-D simulation for varying reactor pressure (C_6H_{12}/O_2, $T_0 = 200$°C, 30% N_2, and $u_0 = 0.194$ m/s).

Lines are model predictions, and symbols are experimental data. (a) O_2, open circles; C_6H_{12}, filled circles; temperature, ×; (b) 5-$C_6H_{10}O$, open circles; C_6H_{10}, filled circles; CO_x, Δ.

Running a simulation at $P = 10$ atm is an attempt to examine predicted reactor behavior at conditions not accessible in the laboratory. High-pressure experiments are costly and potentially dangerous, especially with a reactor constructed from quartz (rather than steel). For a 10-atm reactor pressure, the adiabatic temperature was 846°C, which would mean that chemistry would continue in the presence of oxygen. Conversion of O_2 was predicted to be complete, however, and the C_6H_{12} conversion was 29% (Figure 8a). The product distribution for this simulation included almost 90% selectivity to total oxygenates, with 40% to 5-hexenal and 48% to cyclohexene oxide. The formation of CO and CO_2 became less important (8% selectivity), apparently because gas-phase chemistry dominated at high pressure. This result could be expected, because many of the gas-phase steps are biomolecular (second order in P), while the surface reaction should be first order in P (the flux of oxygen to the surface controls the catalytic step). Additionally, the O_2 diffusivity decreases with pressure (Eq. 18), inhibiting mass transfer to the surface.

The importance of C_6 oxygenates compared to olefins at high pressure is not especially surprising, because the crucial equilibrium between $C_6H_{11}\cdot$ and $C_6H_{11}OO\cdot$ must favor $C_6H_{11}OO\cdot$ as the pressure increases. The rising importance of oxygenates at high pressures is in agreement with many experimental and theoretical studies of alkane oxidation. The reason for the increasing selectivity to cyclohexene oxide, however, is not obvious. The explanation might simply be that the higher temperatures attained at 10 atm open up the β channel along with the γ channel. Another possibility is that the combination of cyclohexene and hydroperoxy radicals (to form β-cyclohexylperoxy radicals) becomes more important.

Turbulence

The possibility of turbulent flow needs to be considered. Hydrodynamic flow normal to an infinite cylinder approximates the flow past a single wire of a high-porosity (such as 40-mesh) screen. At Reynolds numbers less than 0.5, the flow is fully laminar. A slow transition beginning at $Re \approx 0.5$ causes a turbulent wake to develop downstream from the cylinder (Nowak, 1966). This wake flow is fully developed at $Re \approx 100$. The Reynolds number for the experiments lies in the range $Re = 0.5-2$, suggesting that a possible transition to turbulence should be considered. Futhermore, surface roughness can promote the onset of turbulence. However, base-case simulations incorporating turbulent flow and reasonable roughness constants did not yield measurable differences compared to results for pure laminar flow over a smooth wire. It appears that this system can be modeled well with 2-D laminar flow, at least for $u_0 \leq 0.2$ m/s. For higher velocities, the effects of turbulence and surface roughness could become more important.

Radical generation at the surface

A major unanswered question in the single-gauze reactor is the effect of surface-generated radicals and their possible role in speeding up homogeneous chemistry after desorbing into the gas phase. Desorption is favored strongly by high temperatures, such as those attained by the surface. Calculations for varying levels of ·OH originating from the catalyst surface showed that unrealistically high source concentrations of hydroxyl radicals were necessary for a large effect on conversions. The mechanism does not include chain-branching reactions, so the role of ·OH as a chain-reaction carrier is minimal. Certainly, ·OH is much more effective than O_2 for abstracting hydrogen from C_6H_{12}. However, the model calculations do not support ·OH assistance to gas-phase reactions *per se*. A complete mechanism could decrease induction periods. A gas-phase model of *n*-butane partial oxidation in a single-gauze reactor (Iordanoglou and Schmidt, 1998), in fact, did show that radical assistance can substantially speed up homogeneous chemistry.

Discussion and limitations of 2-D model

A 2-D CFD model of the 40-mesh Pt−10%Rh single-gauze catalyst, with 35 reactions among 25 species, was capable of simulating the operation of the reactor reasonably well. By including surface chemistry and conduction in the wire, surface temperatures predicted by the model were consistent with pyrometric measurements. Predicted adiabatic temperatures show that the temperature, measured by a thermocouple 5 mm downstream of the gauze, was always about 50°C less than the adiabatic temperature. The primary reaction zone was small—most of the reactions started and finished within one millisecond, well within the boundaries of the computational grid. In general, the conversions of both cyclohexane and oxygen were underpredicted, which is most likely a result of the assumptions applied to the flow field. Selectivities were in fair agreement with experimental data. The base-case simulation, when compared to the experiment, only failed to accurately describe pentanal (as well as the minor species not present in the model, of course).

Contrary to the 1-D model for which 5-hexenal always dominated the product distribution, the inclusion of the correct geometry and fluid dynamics allowed prediction of cyclohexene (for $C_6H_{12}/O_2 = 4$) or even cyclohexene oxide (for $P = 10$ atm) as the major products. Still, 5-hexenal production was generally higher than that meaured. This result suggests that, if the DFT kinetics are correct, decomposition pathways of 5-hexenal (to CO and $\leq C_5$ olefins and oxygenates, including pentanal) are probably important. 5-Hexenal was maximized in the wake region where temperatures, although falling rapidly, are still high enough for C_6 oxygenates to fall apart.

The equilibrium between cyclohexyl and cyclohexylperoxy radicals was certainly an important factor in determining predicted product selectivities. Low temperatures and high pressures favored $C_6H_{11}OO\cdot$, so $C_6H_{11}\cdot$ (and consequently C_6H_{10} formation) was much more important near the surface. If the equilibrium shifts toward $C_6H_{11}OO\cdot$, parent oxygenates form at the expense of olefins. A big advantage of higher pressure, then, appears to be the high yields to parent oxygenates due to the increased formation of $C_6H_{11}OO\cdot$.

The actual temperature profile is perturbed by the presence of the perpendicular wires, with the magnitude of the perturbation decreasing for larger wire spacings. A 3-D model is therefore expected to yield somewhat different flow fields compared to the 2-D model. The effect of wire crossing (and the disrupted flow pattern in the wake) was also neglected in this model. Finally, the flow does not enter the catalyst region uniformly. The flow in the tube upstream of the gauze screen is laminar, so the velocity and contact time vary across the tube diameter (shorter contact times near the centerline). The underprediction of conversions was most likely a direct result of the assumptions involved in the 3-D → 2-D transformation.

Limitations imposed by the geometry and flow pattern can be irrelevant if the chemistry is wrong. The reactions modeled are a limited set of all the possible reactions. Although the DFT mechanism includes 46 elementary reactions, there really are thousands of reactions and hundreds of species that could be considered. β-Decomposition pathways of the cyclohexylperoxy radical and other oxygen-containing species would lead to many of the $\leq C_4$ species observed experimentally. Decarbonylation reactions of oxygenates, producing CO in the gas phase, might also be important. The DFT mechanism implicitly assumes thermal quenching, because if temperatures remained at or near T_s for long times, species-decomposition pathways would probably dominate the final product distribution. There is an extremely large number of free-radical chain reactions that could be included, and much current research is devoted to the automatic generation of such mechanisms (Chevalier et al., 1990).

Pentanal is the major underpredicted oxygenate, although it is the second-most abundant oxygenate predicted by the model. Because pentanal experimentally decreases in selectivity with pressure, it might not be formed by a bimolecular gas-phase process, as in the proposed reaction scheme. Instead, unimolecular decomposition of 5-hexenal to pentanal could account for the data and help rectify the absence of $C_5H_{10}O$ in the simulations (as well as the overprediction of 5-$C_6H_{10}O$).

The reasonable agreement of the base-case simulation and experimental results suggests that the mechanism, as proposed, was adequate to describe the reactor performance semiquantitatively, especially with the base-case conditions. Some of the trends with operating parameters were slightly incorrect. Furthermore, extensions of the model to conditions outside the experimental window are especially sensitive to errors or omissions in the mechanism. The simulation at 10 atm interestingly predicts close to 90% selectivity to the parent oxygenates 5-hexenal and cyclohexene oxide. However, high pressure should increase the importance of competing gas-phase decomposition pathways not included in the model. The results of the high-pressure simulation were interesting but cannot be regarded as quantitatively correct until the appropriate decomposition pathways are added to the model.

Simplified surface chemistry appears to be sufficient to explain both CO_x selectivities and catalyst surface temperatures. Catalytic formation to pentanal would be a convenient explanation, but there is no experimental evidence for it. There is evidence, on the other hand, for some benzene, ethylene, and butadiene formation on the surface. In order to describe benzene formation, cyclohexane adsorption must be followed by multiple dehydrogenations and then desorption of C_6H_6. Ethylene and butadiene would follow from cracking of adsorbed cyclohexene, which itself could instead desorb as a surface-reaction product. There is no obvious way to lump these reactions, and they are not necessarily mass-transfer limited. DFT calculations of surface reactions are possible (Venkataraman and Neurock, 2000), enabling a challenging future research direction.

Summary of Reactor Simulations

Modeling the single-gauze millisecond reactor for the production of oxygenates and olefins is complicated by several factors, including the interaction of coupled homogeneous−heterogeneous chemistry with mass and heat transfer. The kinetics found by density-functional theory were used in 1-D and 2-D models of the single-gauze reactor. The 1-D model (with 46 reactions and 31 species) assumed plug flow, which placed inherent limitations on the results. A crucial

issue is the rapid thermal gradients near the catalyst wire. Fast quenching of hot unstable intermediates in the wake region of the gauze allows highly nonequilibrium species to be obtained, and this effect is only well-simulated with a two-dimensional geometry. A pseudo−2-D model was developed, using an axial temperature profile suggested by fluid-dynamic calculations. This model allowed reasonable prediction of the conversions in a narrow reaction zone, but selectivities (especially 5-hexenal) were not correct.

A full 2-D model of the 40-mesh Pt−10%Rh single-gauze catalyst, with rigorous fluid dynamics and 35 reactions among 25 species, was capable of simulating the operation of the reactor reasonably well. The 2-D CFD simulations demonstrated that the primary role of the catalyst is to ignite the feed by total oxidation of cyclohexane on the surface, generating heat to initiate homogeneous reactions. Oxygenates form downstream by rearrangement of cyclohexylperoxy radicals. Olefins are produced in parallel to oxygenates, through the cyclohexyl radical that is favored by high temperature and low pressure.

Many limitations of these models have been pointed out. In general, the prediction of conversions in these simulations seems to be governed primarily by the description of the geometry and flow field, while the prediction of selectivities is more affected by the proposed chemical mechanism. Accordingly, a 3-D model could probably allow closer agreement to experimental conversions, while improvements in computed product distributions would likely require a reaction network consisting potentially of hundreds of species and thousands of elementary reactions. Of course, the ultimate model would include 3-D turbulent flow over roughened wires, detailed surface and gas-phase chemistry, transients, surface-radical equilibria, coke formation, and catalyst deactivation.

These calculations do provide fundamental understanding of the favored reaction pathways for cyclohexane partial oxidation in Pt−10%Rh single-gauze reactors and suggest ways to adjust reactor operation for desired product distributions. Numerical simulations of the surface-assisted gas-phase process allow the investigation of experiments that are costly or potentially dangerous to carry out, such as operation's at elevated pressures that are industrially feasible. The 2-D model predicts that high selectivities to the parent oxygenates 5-hexenal and cyclohexene oxide could be viable, as long as side reactions do not invalidate the proposed mechanism.

Vapor-phase high-temperature rapid oxidation followed by fast cooling is a radically different concept for the production of intermediate chemicals. The catalyst contact time is six orders of magnitude smaller than reactor residence times for comparable liquid-phase processes, allowing higher throughputs and thus lower capital costs. The limitation for this technology is arguably that separation of the product stream would be difficult for some applications. If downstream separation proves to be economical, millisecond chemical reactors have tremendous potential. The ultimate success of these reactors will also depend on supporting technologies. For example, a process demonstrating the direct conversion of 5-hexenal to adipic acid would increase the demand and value of 5-hexenal. Cyclohexene is more valuable than cyclohexane, and there are proven applications for cyclohexene oxide, which could be a major product at high pressures. Scale-up and safety will certainly be important issues for commercialization.

Acknowledgments

This research was partially supported by grants from the DOE, the NSF, and DuPont. We wish to thank the Minnesota Supercomputer Institute (MSI) for the generous CPU time provided for the DFT and CFD calculations. Also, we thank Dr. Patton Fast (MSI) and Professor Chris Cramer (University of Minnesota Department of Chemistry) for their advice and assistance on the theoretical considerations of density-functional theory. One of the authors (R.P.O.) gratefully acknowledges Jürgen Warnatz and financial support by the Deutsche Forschungsgemeinschaft (DFG) within the Sonderforschungsbereich 359 for a one-month stay at Heidelberg University.

Literature Cited

Becke, A. D., "Density-Functional Exchange-Energy Approximation with Correct Asymptotic Behavior," *Phys. Rev. A*, **38**, 3098 (1988).

Bharadwaj, S. S., C. Yokoyama, and L. D. Schmidt, "Catalytic Partial Oxidation of Alkanes on Silver in Fluidized Bed and Monolith Reactors," *Appl. Catal. A: Gen.*, **140**, 73 (1996).

Chevalier, C., J. Warnatz, and H. Melenk, "Automatic Generation of Mechanisms for the Description of the Oxidation of Higher Hydrocarbons," *Ber. Bunsenges. Phys. Chem.*, **94**, 1362 (1990).

Chong, D. P., ed., *Recent Advances in Density-Functional Methods*, World Scientific, NJ (1995).

Dietz, A. G., III, and L. D. Schmidt, "Effect of Pressure on Three Catalyst Partial Oxidation Reactions at Millisecond Contact Times," *Catal. Lett.*, **33**, 15 (1995).

Faravelli, T., A. Goldaniga, E. Ranzi, A. Dietz, M. Davis, and L. D. Schmidt, "Partial Oxidation of Hydrocarbons: An Experimental and Kinetic Modeling Study," *Nat. Gas Convers. V — Stud. Surf. Sci. Catal.*, **119**, 575 (1998).

Foresman, J. B., and A. E. Frisch, *Exploring Chemistry with Electronic Structure Methods*, 2nd ed., Gaussian, Inc., Pittsburgh (1996).

Fluent 4.5.2, Fluent Inc., Lebanon, NH (1998).

Gaussian, Inc., Gaussian 98, Rev. A.7, Pittsburgh (2000).

Goestch, D. A., P. M. Witt, and L. D. Schmidt, "Partial Oxidation of Butane at Microsecond Contact Times," *Heterogeneous Hydrocarbon Oxid.*, **1**, 125 (1996).

Iordanoglou, D. I., and L. D. Schmidt, "Oxygenate Formation from *n*-Butane Oxidation at Short Contact Times: Different Gauze Sizes and Multiple Steady States," *J. Catal.*, **176**, 503 (1998).

Iordanoglou, D. I., A. S. Bodke, and L. D. Schmidt, "Production of Chemicals Using Single Gauze Reactors at Short Contact Times," *J. Catal.*, **187**, 400 (1999).

Kang, D. B., and A. B. Anderson, "Theoretical Interpretation of the Cyclohexane → Benzene Reaction on the Pt(111) Surface," *J. Amer. Chem. Soc.*, **107**, 7858 (1985).

Kee, R. J., and Reaction Design, Inc., *CHEMKIN Collection*, Release 3.5, San Diego (1999).

Kryachko, E. S., and E. V. Ludeña, *Energy Density-Functional Theory of Many-Electron Systems*, Kluwer, Boston (1990).

Labanowski, J. K., and J. W. Andzelm, eds., *Density-Functional Methods in Chemistry*, Springer-Verlag, New York (1991).

Larson, R. S., "A Fortran Program for the Analysis of Plug Flow Reactors with Gas-Phase and Surface Chemistry," Sandia National Laboratories Report SAND96-8211, Sandia National Labs., Albuquerque, NM (1996).

Nehse, M., J. Warnatz, and C. Chevalier, "Kinetic Modelling of the Oxidation of Large Aliphatic Hydrocarbons," *Proc. Symp.* (International) on Combustion, p. 773 (1966).

Nowak, E. J., "Catalytic Oxidation of Ammonia on Platinum," *Chem. Eng. Sci.*, **21**, 19 (1966).

O'Connor, R. P., and L. D. Schmidt, "Catalytic Partial Oxidation of Cyclohexane in a Single-Gauze Reactor," *J. Catal.*, **191**, 245 (2000a).

O'Connor, R. P., and L. D. Schmidt, "C_6 Oxygenates from *n*-Hexane in Single-Gauze Reactors," *Chem. Eng. Sci.*, **55**, 5693 (2000b).

Petzold, L. R., "A Description of DASSL," Sandia National Laboratories Report SAND82-8637, Sandia National Labs. (1982).

Ranzi, E., T. Faravelli, P. Gaffuri, E. Garavaglia, and A. Goldaniga, "Primary Pyrolysis and Oxidation Reactions of Linear and Branched Alkanes," *Ind. Eng. Chem. Res.*, **36**, 3336 (1997).

Venkataraman, P. S., and M. Neurock, "Electronic Factors Governing Ethylene Hydrogenation and Dehydrogenation Activity of

Pseudomorphic PdML/Re(0001), PdML/Ru(0001), Pd(111), and PdML/Au(111) Surfaces," *J. Catal.*, **191**, 301 (2000).
Welty, J. R., C. E. Wicks, and R. E. Wilson, *Fundamentals of Momentum, Heat, and Mass Transfer*, 3rd ed., Wiley, New York (1984).
Weast, R. C., ed., *Handbook of Chemistry and Physics*, 64th ed., CRC Press, Boca Raton, FL (1984).
Zeelenberg, A. P., and H. W. de Bruijn, "Kinetics, Mechanism, and Products of the Gaseous Oxidation of Cyclohexane," *Combust. Flame*, **9**, 281 (1965).

Manuscript received July 3, 2001, and revision received Nov. 13, 2001.